Modelling of dendritic growth in ternary alloy solidification with melt convection

D.-K. Sun[1], M.-F. Zhu*[1], T. Dai[1], W.-S. Cao[2], S.-L. Chen[2], D. Raabe[3] and C.-P. Hong[4]

A two-dimensional lattice Boltzmann-cellular automaton model is coupled with the CALPHAD (Calculation of Phase Diagrams) method for simulating dendritic growth during ternary alloy solidification with convection. In the model, the kinetics of dendritic growth is determined by the difference between the equilibrium liquidus temperature and the actual temperature at the solid/liquid interface, incorporating the effects of the interface curvature and the preferred dendritic growth orientation. The lattice Boltzmann method is used for evaluating the local liquid compositions of the two solutes impacted by diffusion and convection. Based on the local liquid compositions, the equilibrium liquidus temperature and the solid concentrations of the two solutes are obtained by the CALPHAD method. The model is applied to simulate dendritic growth of an Al–4·0 wt-%Cu–1·0 wt-%Mg ternary alloy with melt convection. The results demonstrate the high numerical convergence and stability, as well as computational efficiency, of the proposed model. Melt convection is found to influence the dendritic morphologies and microsegregation patterns in the solidification of ternary alloys.

Keywords: Modelling, Lattice Boltzmann method, Cellular automaton, Dendritic growth, Convection, Ternary alloy

This paper is part of a special issue of papers selected from MCSP8, the 8th Pacific Rim Conference on Modeling of Casting and Solidification Processes

Introduction

Microstructure and microsegregation developed in solidification are closely associated with the properties of final products. As most commercial materials are multicomponent alloys and the analysis of solidification in multicomponent alloys is much more difficult than that in binary alloys, research on the microstructure and microsegregation evolution in multicomponent alloy solidification has received increasing interest.[1] In addition, melt convection is known as an unavoidable phenomenon in solidification process, which alters the thermal and solutal transport and thus impacts the evolution of solidification microstructures.

With the rapid development of powerful computers and advanced numerical techniques, numerical modelling has emerged as an important and indispensable tool for the research of solidification. Various numerical approaches are proposed to simulate the evolution of microstructure and microsegregation, which involves the effects of melt flow, thermal/solutal transport, dendrite coarsening, capillary effects, ..., preferential crystal orientation, thermodynamics and kinetics on the moving solid/liquid (SL) interface. Models based on the cellular automaton (CA) technique can reproduce a wide range of microstructure features observed experimentally with an acceptable computational efficiency, indicating the excellent potential for engineering applications.[2–5] Some of the present authors developed a CA model that is coupled with PanEngine that is the kernel part of a thermodynamic and phase equilibrium calculation software package PANDAT[6] for the prediction of microstructures and microsegregation in the solidification of ternary alloys for the case of pure diffusion.[7] Two of the present authors further extended the model to the system including melt convection by combining the CA-PanEngine model with a Navier–Stokes (NS) solver.[8] The model is able to simulate dendritic growth behaviour in ternary alloy solidification in the presence of convection. However, as the NS solver is a continuum based approach and limited in implementing non-slip boundary conditions at the moving SL interface, the fluid flow calculation becomes difficult to converge as the solid fraction increases. It is found that when the solid fraction reaches ~0·3, the simulation encounters convergence problems of the fluid flow calculation.

During the last two decades, the lattice Boltzmann method (LBM) has rapidly developed as a new powerful tool for the numerical calculation of fluid flow, heat and solute transport. Lattice Boltzmann method is a kinetic approach that considers flows to be composed of a collection of pseudoparticles represented by a distribution function.[9–13] Compared to conventional computational

[1]Jiangsu Key Laboratory for Advanced Metallic Materials, School of Materials Science and Engineering, Southeast University, Nanjing 211189, China
[2]CompuTherm LLC, 437 S. Yellowstone Dr, Suite 217, Madison, WI 53719, USA
[3]Max-Planck-Institut fur Eisenforschung, Düsseldorf 40237, Germany
[4]Center for Computer-Aided Materials Processing (CAMP), Department of Metallurgical Engineering, Yonsei University, Seoul 120749, Korea

*Corresponding author, email zhumf@seu.edu.cn

© 2011 W. S. Maney & Son Ltd.
Received 2 July 2010; accepted 25 October 2010
DOI 10.1179/136404611X13001912813988

fluid dynamics, LBM has the merits of high computational efficiency, good versatility in the constitutive description of its underlying pseudoparticles and simplicity in coding. In particular, LBM exhibits good numerical stability for simulating complex fluid systems, such as multiphase and multicomponent flow phenomena under complicated geometrical boundary conditions. Since LBM describes fluid motion at the level of the distribution functions, it can be naturally incorporated with the related simulation techniques for crystal growth in a fluid flow. Miller *et al.*[14] and Medvedev *et al.*[15] developed phase field LBM coupled models for the simulation of convective dendritic growth in pure substances. Recently, some of the present authors suggested a CA based approach coupled to an LBM solver for simulating the dendrite growth of binary alloys in the presence of forced convection.[16,17]

In this paper, the previously developed two-dimensional (2D) LBM-CA model[17] is extended to the ternary alloy system by coupling the model with the thermodynamic software package PanEngine for the simulation of dendritic growth during ternary alloy solidification in the presence of melt convection. The model details, validations through the comparison of the simulations to the analytical predictions and simulated dendritic morphologies of an Al–4·0 wt-%Cu–1·0 wt-%Mg ternary alloy with forced flow are presented.

Governing equations and numerical algorithm

Model description

In the present work, the LBM with the lattice Bhatnagar–Gross–Krook scheme[11,12] is adopted for the calculation of melt convection and solute transport. Since in the solid phase there is no convection, and the solute transport is purely governed by diffusion, the finite difference method (FDM) is applied to solve the solute diffusion in the solid phase. The diffusion coefficients in solid and liquid are considered to be independent of composition but temperature dependent. Two solutes are considered to diffuse independently, and cross-diffusion is neglected. In addition, since the thermal diffusivity of Al rich alloys is about four orders of magnitudes larger than the solute diffusivity, the kinetics for dendritic growth can be assumed to be solute transport controlled. In the present work, the temperature field in the domain is considered to be uniform with a constant undercooling or cooling down from the liquidus with a constant cooling rate. Based on the domain temperature and the LBM calculated local liquid compositions of two solutes, which are controlled by both convection and diffusion, the kinetics of dendritic growth is determined by a CA approach. Two of the key parameters required in the microstructure modelling of alloys are the solute partition coefficient and the liquidus slope. For simple binary alloy systems, they are usually considered to be suitably taken as constants. However, for multicomponent systems, these two parameters may vary significantly with temperature and compositions. Accordingly, it is necessary to couple microstructure simulation models with thermodynamic calculations in the modelling of the microstructure and microsegregation of multicomponent alloys. In the present work, the CA approach is coupled with PanEngine that is developed based on the CALPHAD method[6] to obtain phase equilibrium information of the ternary alloy systems. The governing equations and numerical algorithms for calculating fluid flow, solute field, interface curvature, crystallographic anisotropy and growth kinetics are described below.

Calculation of fluid flow and solute transport

In the present work, LBM is adopted for numerically calculating fluid flow by solving the discrete Boltzmann equation on a lattice. According to the Bhatnagar–Gross–Krook approximation, the lattice Boltzmann equation (LBE) can be expressed as[11,12]

$$f_i(\boldsymbol{x}+\boldsymbol{e_i}\Delta t,t+\Delta t)-f_i(\boldsymbol{x},t)=-[f_i(\boldsymbol{x},t)-f_i^{eq}(\boldsymbol{x},t)]/\tau \quad (1)$$

where $f_i(\boldsymbol{x},t)$ is the particle distribution function (PDF) representing the probability of finding a particle at location $\boldsymbol{x}$ at time t, $\boldsymbol{e_i}$ is the discrete moving velocity of the pseudoparticle, Δt is the time step, τ is the relaxation time and $f_i^{eq}(\boldsymbol{x},t)$ is the equilibrium PDF (EPDF).

Lattice Boltzmann method can also be used to simulate solute transport due to convection and diffusion. Similar to the LBE for fluid flow calculation, the LBE for solute transport with PDF $g_i^\sigma(\boldsymbol{x},t)$ and source term $G_i^\sigma(\boldsymbol{x},t)$ can be written as[13]

$$g_i^\sigma(\boldsymbol{x}+\boldsymbol{e_i}\Delta t,t+\Delta t)-g_i^\sigma(\boldsymbol{x},t)= -[g_i^\sigma(\boldsymbol{x},t)-g_i^{\sigma,eq}(\boldsymbol{x},t)]/\tau_D^\sigma+G_i^\sigma(\boldsymbol{x},t) \quad (2)$$

where the superscript 'σ' stands for the σth component of alloys ($\sigma=1,2$). τ_D^σ and $g_i^{\sigma,eq}(\boldsymbol{x},t)$ are the relaxation times and the EPDFs for the transport of two solutes, respectively. The source term, $G_i^\sigma(\boldsymbol{x},t)$ in equation (2) denotes the rejected solute contents of the σth component during dendritic growth.

A 2D nine-velocity (D2Q9) scheme[11,12] is employed, where space is discretised into a square lattice, including nine discrete velocities $\boldsymbol{e_i}$, given as

$$\boldsymbol{e_i}=\begin{cases}(0,0), & i=0\\ (\cos[(i-1)\pi/2],\sin[(i-1)\pi/2])c, & i=1-4\\ (\cos[(2i-9)\pi/4],\sin[(2i-9)\pi/4])2^{1/2}c, & i=5-8\end{cases} \quad (3)$$

where $c=\Delta x/\Delta t$ is the lattice speed, and Δx is the lattice spacing. Macroscopic variables such as fluid density ρ, velocity $\boldsymbol{u}$ and concentration C^σ can be calculated from the relevant PDFs, respectively

$$\rho=\sum_{i=0}^{8} f_i,\ \rho\boldsymbol{u}=\sum_{i=0}^{8} f_i\boldsymbol{e_i} \text{ and } C^\sigma=\sum_{i=0}^{8} g_i^\sigma \quad (4)$$

In the D2Q9 scheme of LBM, the EPDFs in equations (1) and (2) are defined as

$$f_i^{eq}(\boldsymbol{x},t)=w_i\rho\left[1+3\frac{(\boldsymbol{e_i}\cdot\boldsymbol{u})}{c^2}+4.5\frac{(\boldsymbol{e_i}\cdot\boldsymbol{u})^2}{c^4}-1.5\frac{\boldsymbol{u}^2}{c^2}\right] \quad (5)$$

$$g_i^{\sigma,eq}(\boldsymbol{x},t)=w_iC^\sigma\left[1+3\frac{(\boldsymbol{e_i}\cdot\boldsymbol{u})}{c^2}+4.5\frac{(\boldsymbol{e_i}\cdot\boldsymbol{u})^2}{c^4}-1.5\frac{\boldsymbol{u}^2}{c^2}\right] \quad (6)$$

where w_i are the weight coefficients given by $w_0=4/9$, $w_{1-4}=1/9$ and $w_{5-8}=1/36$. According to the Chapman–Enskog analysis, the kinematic viscosity v and the solutal diffusivities in liquid D_l^σ are related to the relaxation times τ and τ_D^σ respectively

$$v=c^2\Delta t(2\tau-1)/6 \text{ and } D_l^\sigma=c^2\Delta t(2\tau_D^\sigma-1)/6 \quad (7)$$

In the solid phase, no flow occurs, and solute transport occurs via diffusion only. The solute diffusion is governed by the following equation that is solved using an explicit finite difference scheme

$$\frac{\partial C_{\mathrm{s}}^{\sigma}}{\partial t}=\nabla\left(D_{\mathrm{s}}^{\sigma}\nabla C_{\mathrm{s}}^{\sigma}\right)\ (\sigma=1,\,2) \tag{8}$$

To calculate the unknown PDFs at the boundary nodes of a 2D domain $[(x,\,y)|0\leqslant x\leqslant L,\,0\leqslant y\leqslant L]$, the following boundary conditions are adopted. The undercooled melt flows into the domain from the left surface with a uniform inlet velocity $\boldsymbol{u}(x,y)|_{\mathrm{x}=0}=(U_{\mathrm{in}},0)$ and flows out from the right wall with $\partial_{\mathrm{x}}u_{\mathrm{x}}|_{\mathrm{x}=\mathrm{L}}=0$. The non-equilibrium extrapolation scheme[18] is used to treat the inlet and outlet boundaries, whereas the periodic boundary conditions are imposed on the top and bottom walls. Since there is no convection in solid, and solute transport at the SL interface is neglected, the bounce back scheme is applied at the SL interface for both fluid flow and solute field calculation. The zero flux boundary condition of $\partial_{\mathrm{x}}C|_{\mathrm{x}=0,\mathrm{L}}=0$ and $\partial_{\mathrm{y}}C|_{\mathrm{y}=0,\mathrm{L}}=0$ for solute transfer is implemented on the four surfaces of the calculation domain.

Solution of phase fraction evolution

Dendritic growth is considered to be driven by the local undercooling. The local undercooling at time t, $\Delta T(t)$, is defined as the difference between the local equilibrium liquidus temperature and the local actual temperature, incorporating the curvature effect of the SL interface, and it is expressed as

$$\Delta T(t)=T^{*}(t)-T(t)-\Gamma(\theta)K(t) \tag{9}$$

where $T^{*}(t)$ is the local equilibrium liquidus temperature obtained from PanEngine, which derives it based on the local liquid compositions of two solutes, $T(t)$ is the local actual temperature determined by the imposed undercooling or cooling rate, $\Gamma(\theta)$ is the Gibbs–Thomson coefficient incorporated with the effect of the anisotropy of the surface energy and $K(t)$ is the local interface curvature that is calculated according to the gradient of local solid fraction at the interface using the following equation

$$\begin{aligned}K(t)=&\left[2\partial_{\mathrm{x}}f_{\mathrm{s}}\partial_{\mathrm{y}}f_{\mathrm{s}}\partial_{\mathrm{xy}}^{2}f_{\mathrm{s}}-(\partial_{\mathrm{x}}f_{\mathrm{s}})^{2}\partial_{\mathrm{y}}^{2}f_{\mathrm{s}}-(\partial_{\mathrm{y}}f_{\mathrm{s}})^{2}\partial_{\mathrm{x}}^{2}f_{\mathrm{s}}\right]\\&\times\left[(\partial_{\mathrm{x}}f_{\mathrm{s}})^{2}+(\partial_{\mathrm{y}}f_{\mathrm{s}})^{2}\right]^{-3/2}\end{aligned} \tag{10}$$

where f_{s} is the local solid fraction. The growth velocity and the local undercooling is related by

$$V_{\mathrm{g}}(t)=\mu_{\mathrm{k}}(\theta)\Delta T(t) \tag{11}$$

where $V_{\mathrm{g}}(t)$ is the interface growth velocity, and $\mu_{\mathrm{k}}(\theta)$ is the interface kinetic coefficient.

Since dendrites typically grow with specific preferred crystallographic orientations, it is necessary to consider crystalline anisotropy in either the surface energy or the interfacial kinetics (or both) in the model of dendritic growth.[19] The present model accounts for the anisotropy in both surface energy and interfacial kinetics. For an fcc lattice crystal of Al rich alloys simulated in the present work, it exhibits the fourfold anisotropy of the surface energy and kinetics at the SL interface. The Gibbs–Thomson coefficient $\Gamma(\theta)$ and the interface kinetics coefficient $\mu_{\mathrm{k}}(\theta)$ are given by

$$\Gamma(\theta)=\bar{\Gamma}\{1-15\varepsilon\cos[4(\theta-\theta_{0})]\} \tag{12}$$

$$\mu_{\mathrm{k}}(\theta)=\bar{\mu}_{\mathrm{k}}\{1+\delta_{\mathrm{k}}\cos[4(\theta-\theta_{0})]\} \tag{13}$$

where $\bar{\Gamma}$, ε, $\bar{\mu}_{\mathrm{k}}$ and δ_{k} are the average Gibbs–Thomson coefficient, the degree of anisotropy of the surface energy, the average interface kinetic coefficient and the degree of kinetic anisotropy respectively. θ is the angle between the normal of the SL interface and the horizontal direction, and θ_0 is the preferred dendrite growth orientation. The angle θ is calculated according to the gradient of the solid fraction at the SL interface by

$$\theta=\arctan\left(\frac{\dfrac{\partial f_{\mathrm{s}}}{\partial y}}{\dfrac{\partial f_{\mathrm{s}}}{\partial x}}\right) \tag{14}$$

The growth velocities of interface cells are calculated with equations (9)–(14). The change rate of solid fraction of an interface cell can thus be evaluated from the growth velocity $V_{\mathrm{g}}(t)$ as follows

$$\frac{\partial f_{\mathrm{s}}}{\partial t}=G\frac{V_{\mathrm{g}}}{\Delta x} \tag{15}$$

where G is a geometrical factor related to the state of neighbour cells, which is defined by

$$G=\min\left(1,\frac{1}{2}\sum\nolimits_{\mathrm{m}=1}^{4}s_{\mathrm{m}}^{\mathrm{I}}+\frac{1}{2^{1/2}}\sum\nolimits_{\mathrm{m}=1}^{4}s_{\mathrm{m}}^{\mathrm{II}}\right) \tag{16}$$

where S^{I} and S^{II} indicate the state of the nearest neighbour cells and the second nearest neighbour cells respectively. According to the state of a neighbour cell, S^{I} and S^{II} are determined by

$$s^{\mathrm{I}},s^{\mathrm{II}}=\begin{cases}0, & (f_{\mathrm{s}}<1)\\ 1, & (f_{\mathrm{s}}=1)\end{cases} \tag{17}$$

If at time $t=t_{\mathrm{n}}$ the sum of the solid fraction in an interface cell is equal to one, the state of this cell is assigned as solid, and new interface cells are explicitly captured. However, the exact SL front is scaled by the solid fraction within each interface cell.

It is assumed that the local thermodynamic equilibrium is maintained at the SL interface, and thus, the solidified cells always adopt the equilibrium value of the solid concentration. As the dendrite grows, the growing cells reject solutes at the SL interface. The rejected amount of a solute element σ is evaluated by

$$\Delta C^{\sigma}=\Delta f_{\mathrm{s}}\left(C_{\mathrm{l}}^{*,\sigma}-C_{\mathrm{s}}^{*,\sigma}\right) \tag{18}$$

where Δf_{s} is the solid fraction increment of the interface cell at one time step, which is evaluated by equation (15), and $C_{\mathrm{l}}^{*,\sigma}$ and $C_{\mathrm{s}}^{*,\sigma}$ are the interface liquid and solid compositions of solute element σ respectively. The rejected ΔC^{σ} is added to the remaining liquid in the same cell and its surrounding neighbour cells. Thus, the source term $G_{\mathrm{i}}^{\sigma}(x,t)$ in equation (2) can be calculated with $G_{\mathrm{i}}^{\sigma}(x,t)=w_{\mathrm{i}}\Delta C^{\sigma}$. The interface solid compositions of two solutes $C_{\mathrm{s}}^{*,\sigma}$ ($\sigma=1,\,2$) in equation (18) and the interface equilibrium liquidus temperature $T^{*}(t)$ in equation (9) are obtained from PanEngine according to the local interface liquid compositions of two solutes $C_{\mathrm{l}}^{*,1}$ and $C_{\mathrm{l}}^{*,2}$, which are determined using the LBM by

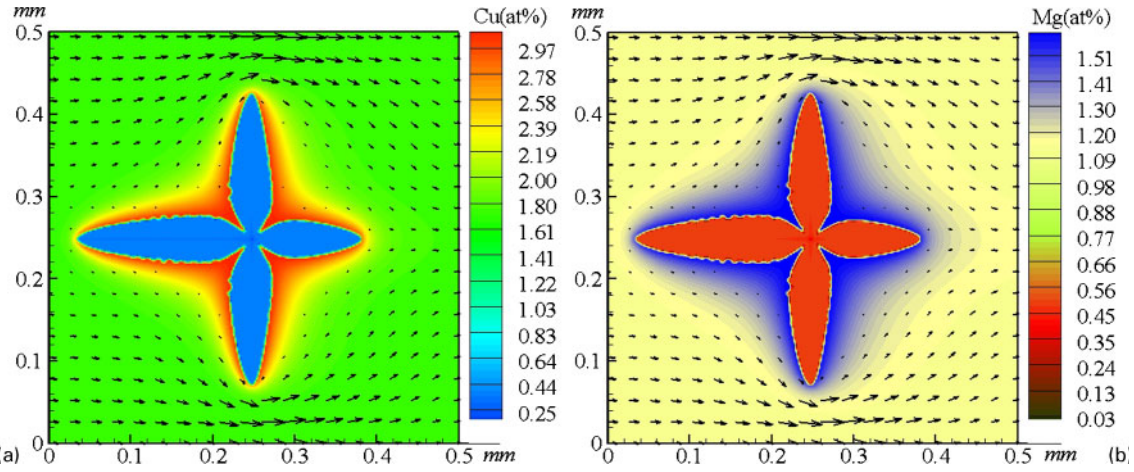

1 Simulated dendritic morphology shown in *a* Cu and *b* Mg compositions of Al–4·0 wt-%Cu–1·0 wt-%Mg alloy grown in flowing melt with $U_{in}=1{\cdot}0\times10^{-3}$ m s^{-1} and $\Delta T=10$ K: velocity vector plots indicate strength and direction of flow

solving equations (1)–(7). To improve the computational efficiency, a data tabulation coupling strategy between CA and PanEngine is adopted. Before starting the CA microstructure simulation, a data file is generated by PanEngine. In the data file, the equilibrium liquidus temperatures and the equilibrium solid compositions are tabulated with respect to the relevant liquid compositions for a uniform grid spacing of 1 at-%. PanEngine can perform the thermodynamic and phase equilibrium calculations based on the Scheil model and the equilibrium model. In this work, the Scheil model is adopted to calculate the data in the tabulation file. During the CA simulation, the required data of equilibrium liquidus temperature and interface solid compositions are interpolated from the data stored in the tabulation grids. The physical parameters used in the present work are taken from Refs. 7 and 20.

Results and discussion

Single dendritic growth

To simulate single dendrite growth in an undercooled melt with forced convection, the calculation was performed on a square domain of 250×250 mesh with a uniform mesh size of $\Delta x=2{\cdot}0$ μm. At the beginning of the simulation, a solid seed with a crystallographic orientation of 0° with respect to the horizontal direction was placed at the centre of the domain. The other cells in the domain were filled with the undercooled liquid with $\Delta T_0=10$ K. The relaxation times for fluid flow and solute transport of Cu and Mg, the time step, the degree of anisotropy of the surface energy and the degree of kinetics anisotropy were taken as $\tau=1{\cdot}0$, $\tau_D^{Cu}=0{\cdot}541$, $\tau_D^{Mg}=0{\cdot}57$, $\Delta t=1{\cdot}17\times10^{-5}$s, $\varepsilon=0{\cdot}02$ and $\delta_k=0{\cdot}3$ respectively. The average interface kinetic coefficient was determined using an inverse problem approach and was taken as $\bar{\mu}_k=3\times10^{-4}$ m s^{-1} K^{-1}.[7] Figure 1 presents the simulated dendrite morphology of an Al–4·0 wt-%Cu–1·0 wt-%Mg alloy growing in forced flow with an inlet flow velocity of $U_{in}=1{\cdot}0\times10^{-3}$ m s^{-1}, which is shown in Cu (Fig. 1*a*) and Mg (Fig. 1*b*) composition maps. It can be noted that the dendritic shape is obviously influenced by fluid flow. The growth of the dendrite is promoted on the upstream side and inhibited on the downstream side. As the dendrite grows, two solutes are released at the SL interface, which are washed away from the upstream to the downstream direction by fluid flow, resulting in asymmetrical solute profiles in the liquid, i.e. the concentrations in the upstream region are lower than in downstream. Figure 2 shows the composition profiles of solutes Cu and Mg along the horizontal dendrite arms with various solid fractions. It can be seen that at the SL interface, there is a sudden increase in compositions of both solutes, which then decay exponentially until they again approach the initial compositions. It can be noted that the liquid compositions at the interface of the downstream tip (on the right hand side) are higher than that of the upstream tip (on the left hand side). The lower local solute concentrations will yield a higher equilibrium liquidus temperature $T^*(t)$. According to equation (9), under a uniform temperature field $T(t)$, the

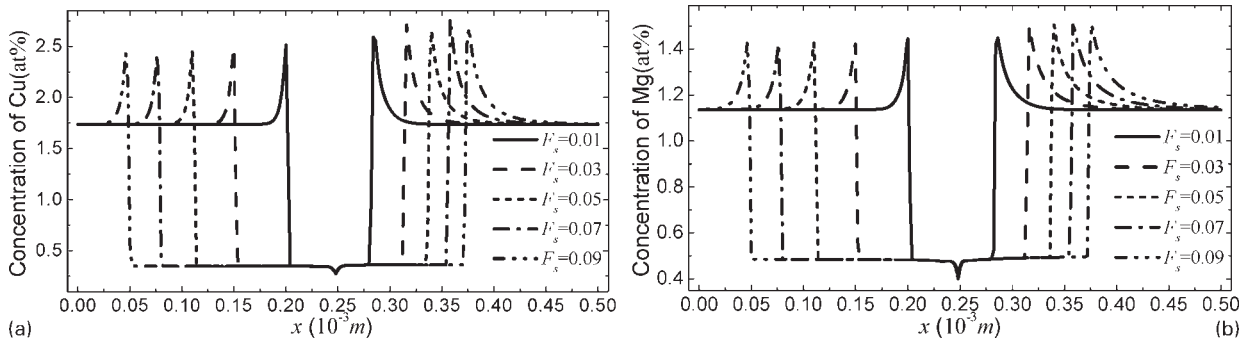

2 Concentration profiles of solutes *a* Cu and *b* Mg along horizontal dendrite arms with various solid fractions (F_s: total solid volume fraction in domain)

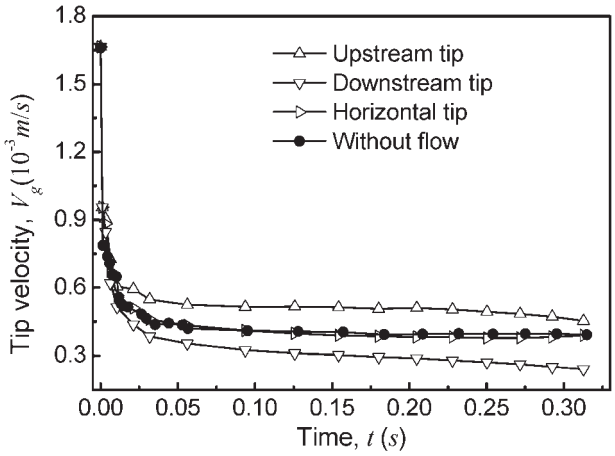

3 Time histories of tip velocities for case of Fig. 1

higher the equilibrium liquidus temperature, the larger the local undercooling. Therefore, the driving force for dendrite growth in the upstream region is larger than that in the downstream region, resulting in an asymmetric dendritic growth morphology.

Figure 3 shows the time history of the tip velocity measured from the dendrite growth in Fig. 1. The tip velocity of pure dendrite growth is also plotted for comparison. As shown, the tip velocity initially rapidly decreases. After a transient period, the velocities of the different tips reach the approximately stable values with different levels. The velocities of the up- and downstream tips are higher and lower than that without flow respectively. The perpendicular tip approaches to an approximately steady state growth velocity that is nearly the same as the case of pure diffusion.

Multidendritic growth

To validate the present model for the simulations of multidendritic solidification, the simulated solute distributions in the solid for the case of pure diffusion are compared with the Scheil model predictions. The calculation domain consisted of 250×250 meshes with $\Delta x = 2$ μm. The temperature in the entire domain was assumed to be uniform and cooled down from liquidus temperature to 600 K with a constant cooling rate of 1 K s^{-1}. The Scheil model assumes no diffusion in solid and complete mixing in liquid. To analyse the effect of diffusion in the solid on the microsegregation, zero and non-zero solid diffusivities were used in the simulations. The simulated concentration profiles of the two solutes as a function of solid fraction are compared with the Scheil predictions in Fig. 4. The Scheil profiles in Fig. 4 were calculated using the phase diagram calculation software PANDAT.[6] Note that the simulated profiles with zero solid diffusivity are almost superimposed on the Scheil profiles for both solutes Cu and Mg. The reasons are as follows. First, as mentioned in the section on 'Solution of phase fraction evolution', the thermodynamic and phase equilibrium calculations using PanEngine are based on the Scheil model. Second, the slow solidification rate of 1 K s^{-1} provides enough time for solute diffusion in liquid, resulting in an almost uniform liquid composition field. Together with the zero solid diffusivity, the simulation conditions are very close to the Scheil assumptions. On the other hand, Fig. 4 also reveals that the calculated solid composition distributions with non-zero solid diffusivities are more homogeneous than those

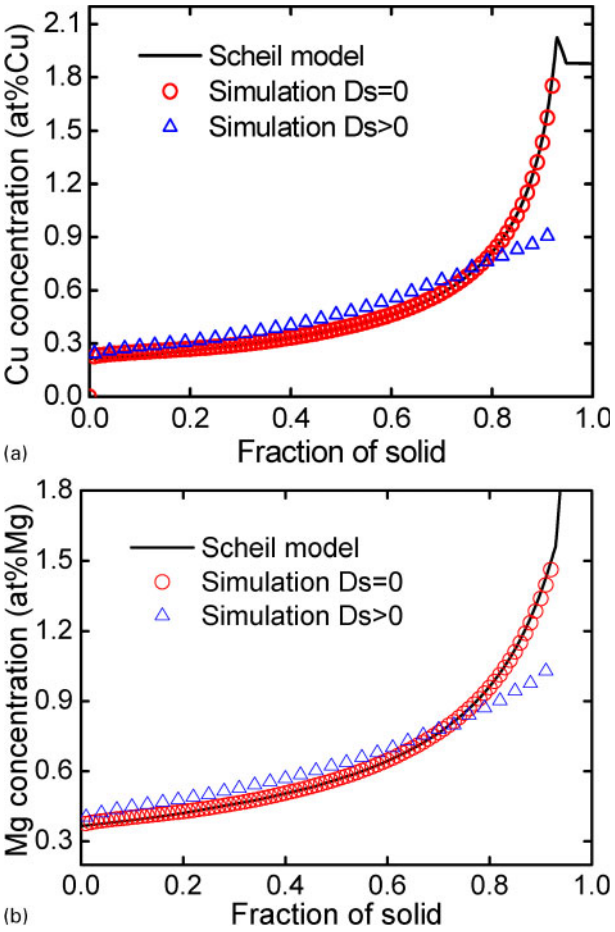

4 Concentration profiles of *a* Cu and *b* Mg solutes as function of solid fraction for Al–4·0 wt-%Cu–1·0 wt-%Mg alloy solidified with cooling rate of 1·0 K s^{-1}: simulation was terminated at T=600 K

obtained with zero solid diffusivity, illustrating the effect of back diffusion on microsegregation.

The proposed model was then applied to simulate the multidendritic growth behaviour with melt convection. Figure 5 presents the simulated evolution of multiequiaxed dendrites of an Al–4·0 wt-%Cu–1·0 wt-%Mg alloy in a flowing melt with $U_{in} = 1{\cdot}0 \times 10^{-3}$ m s^{-1} and a cooling rate of 10 K s^{-1}. For this simulation, the relaxation time for the fluid flow calculation was taken as $\tau = 1{\cdot}0$. Since the diffusivities of two solutes are temperature dependent, the relaxation times for solute transport calculation τ_D^{Cu} and τ_D^{Mg} were also temperature dependent and determined by equation (7). The simulation was stopped at a total solid fraction of 0·93. Figure 5 shows that at the early stage of solidification, melt flows from left to right smoothly along the small dendrites, during which the solute is transported from the upstream side to the downstream side of each dendrite, resulting in asymmetric dendrite features. As solidification proceeds, the primary arms grow and coarsen with the evolution of side branches. The growth of the primary and secondary arms is all distinctly promoted on the upstream direction. Fluid flow almost vanishes in the interdendritic region as the dendrites grow close to each other. Thus, at the later stage, the growth of dendrites is not affected much by flow. However, the final microstructure maintains the deflected dendritic features that were developed in the

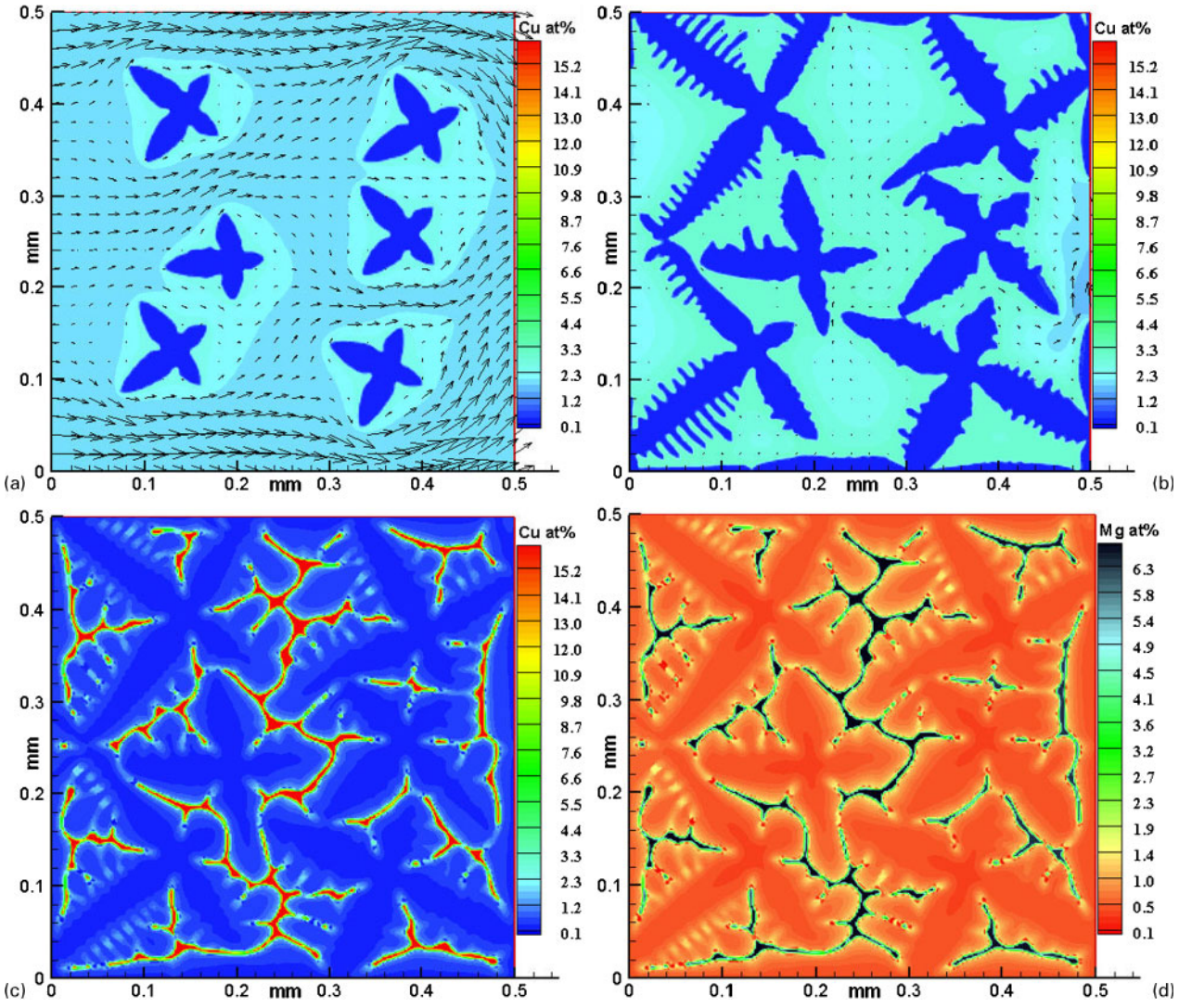

a F_s=0·1; *b* F_s=0·4; *c* F_s=0·93; *d* F_s=0·93

5 Evolution of multidendrites for Al–4·0 wt-%Cu–1·0 wt-%Mg alloy solidified in flowing melt with $U_{in}=1{\cdot}0\times10^{-3}$ m s^{-1} and cooling rate of 10 K s^{-1}: *a–c* composition map of Cu, and *d* composition map of Mg (F_s: total solid volume fraction in domain)

early solidification stage. It can also be noted from Fig. 5 that the proposed model is able to simulate the convective dendrite growth to the end of solidification, i.e. no convergence problem occurs.

The previously developed CA-FDM-PanEngine[7] and CA-NS-PanEngine[8] models were also adopted to simulate pure diffusive and convective dendrites with the same conditions as used in Fig. 5. The time histories of the solid fraction evolution simulated from different models are compared in Fig. 6. It can be observed from Fig. 6*a* that the two sets of data simulated from the CA-LBM-PanEngine and CA-FDM-PanEngine models for pure diffusive dendrite growth agree well with each other. This indicates that the LBE for solute transport calculation is equivalent to Fick's law. On the other hand, as shown in Fig. 6*b*, the evolution of solid fraction with time simulated by the CA-LBM-PanEngine model coincides well with that by the CA-NS-PanEngine when the solid fraction is below 0·24, illustrating that the LBE for fluid flow calculation converges to the NS equation. It is noted that the CA-NS-PanEngine simulation could not proceed when the solid fraction is above 0·24 owing to the convergence problems of the NS solver. However, the present CA-LBM-PanEngine model can perform the simulation of convective dendrite growth to the end of solidification, as shown in Figs. 5 and 6*b*. Accordingly, the present CA-LBM-PanEngine model exhibits better numerical stability than the CA-NS-PanEngine model for simulating dendritic growth of ternary alloys in the presence of melt convection. In addition, the present model is more computationally efficient than the CA-NS-PanEngine model. The calculation times for the convective multidendritic growth (Fig. 6*b*) with total solid fraction F_s in the domain F_s=0·24 is ~43 and 63 min for the CA-LBM-PanEngine and CA-NS-PanEngine models respectively on a PC Core 2 Duo 2·66 GHz CPU.

Conclusions

A coupled CA-LBM-PanEngine model has been developed for simulating the dendrite structure and microsegregation during solidification of ternary alloys in the presence of forced melt convection. In the model, instead of a continuum NS solver, the kinetic based LBM is adopted to model melt flow and solute transport

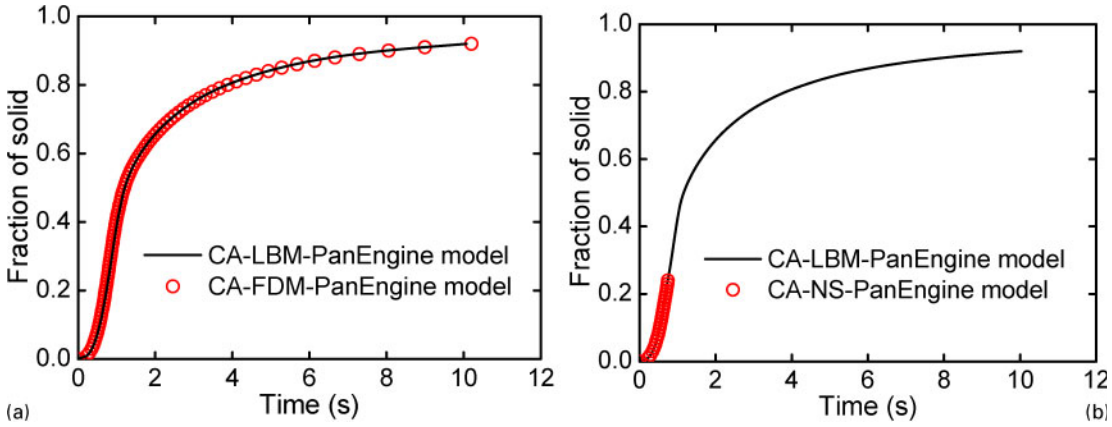

6 Comparisons of solid fraction profiles as function of time simulated by different models for cases of *a* pure diffusive dendrite growth and *b* convective dendrite growth

in the liquid, while the solute diffusion in solid is solved by an explicit finite difference scheme. Dendritic growth is simulated using a CA approach that includes time dependent calculations for the solute redistribution in liquid and solid phases, interface curvature, preferred crystallographic orientations and growth kinetics. The evolution of the SL interface is considered to be driven by the difference between the local equilibrium liquidus temperature and the local actual temperature, incorporating the effect of curvature. Based on the interface liquid compositions of the two solutes, which are determined by the LBM calculations, the local equilibrium liquidus temperature and the interface solid compositions of the two solutes are obtained with the aid of the thermodynamic calculation software package PanEngine. The proposed CA-LBM-PanEngine model was applied to simulate the single dendritic growth of an Al–4·0 wt-%Cu–1·0 wt-%Mg alloy in a forced flow. The tip velocity is found to be enhanced in the upstream region and inhibited in the downstream regions, resulting in the asymmetric growth features of convective dendrites. The model validation for multidendritic simulation was performed by comparing the simulated composition profiles of two solutes in solidified dendrites with the predictions of the Scheil model. The results show that the simulated solid compositions with zero solid diffusivity and low cooling rate of 1 K s^{-1} coincide with the Scheil profiles. Moreover, the calculated solid composition profiles with non-zero solid diffusivities are initially higher and later lower than those obtained with zero solid diffusivity, indicating the effect of back diffusion. The evolution of multiequiaxed dendrites with various orientations in the presence of forced convection was simulated. It is found that at the early stage of solidification, the primary arms and side branches are distinctly deflected towards the incoming fluid flow, whereas the flow effect on dendritic growth gradually fades out at the later stage as the dendrites grow close to each other. The profiles of solid fraction versus time for pure diffusive and convective dendrite growth simulated by the CA-LBM-PanEngine model agree well with those from the previously developed CA-FDM-PanEngine and CA-NS-PanEngine models. It is also shown that the proposed CA-LBM-PanEngine model is numerically more stable and computationally more efficient as well as simpler to be implemented than the CA-NS-PanEngine model for the simulation of dendrite growth of ternary alloys in the presence of melt convection.

Acknowledgements

This work was supported by the National Natural Science Foundation of China (grant no. 50671025 and no. 50971042) and the Specialized Research Fund for the Doctoral Program of Higher Education of China (grant no. 20070286021).

References

1. U. Hecht, L. Gránásy, T. Pusztai, B. Böttger, M. Apel, V. Witusiewicz, L. Ratke, J. D. Wilde, L. Froyen, D. Camel, B. Drevet, G. Faivre, S. G. Fries, B. Legendre and S. Rex: *Mater. Sci. Eng.*, 2004, **46**, R1–R49.
2. L. Belteran-Sanchez and D. M. Stefanescu: *Metall. Mater. Trans. A*, 2004, **35A**, 2471–2485.
3. Y. Liu, Q. Y. Xu and B. C. Liu: *Tsinghua Sci. Technol.*, 2006, **11**, 495–500.
4. M. F. Zhu, C. P. Hong, D. M. Stefanescu and Y. A. Chang: *Metall. Mater. Trans. A*, 2007, **38A**, 517–524.
5. L. Yuan and P. D. Lee: *Modell. Simul. Mater. Sci. Eng.*, 2010, **18**, 055008.
6. S. L. Chen, S. Daniel, F. Zhang, Y. A. Chang, X. Y. Yan, F. Y. Xie, R. Schmid-Fetzer and W. A. Oates: *CALPHAD*, 2002, **26**, (2), 175–188.
7. M.-F. Zhu, W. Cao, S.-L. Chen, C.-P. Hong and Y. A. Chang: *J. Phase Equilib. Diffus.*, 2007, **28**, (1), 130–138.
8. C. P. Hong, M. F. Zhu and S. Y. Lee: *FDMP*, 2006, **2**, (4), 247–260.
9. D. Raabe: *Modell. Simul. Mater. Sci. Eng.*, 2004, **12**, R13–R46.
10. L.-S. Luo: *Phys. Rev. E*, 2000, **62E**, 4982–4996.
11. S. Chen, H. Chen, D. Martinez and W. H. Matthaeus: *Phys. Rev. Lett.*, 1991, **67**, 3776–3779.
12. Y. H. Qian, D. d'Humières and P. Lallemand: *Europhys. Lett.*, 1992, **17**, 479–484.
13. B. Deng, B. C. Shi and G. C. Wang: *Chin. Phys. Lett.*, 2005, **22**, 267–270.
14. W. Miller, I. Rasin and F. Pimentel: *J. Cryst. Growth*, 2004, **266**, 283–288.
15. D. Medvedev, T. Fischaleck and K. Kassner: *J. Cryst. Growth*, 2007, **303**, 69–73.
16. D. K. Sun, M. F. Zhu, S. Y. Pan and D. Raabe: *Acta Mater.*, 2009, **57**, 1755–1767.
17. D. K. Sun, S. Y. Pan, M. F. Zhu and D. Raabe: *Int. J. Mod. Phys. B*, 2009, **23B**, (6–7), 1609–1614.
18. Z.-L. Guo, C.-G. Zheng and B.-C. Shi: *Chin. Phys.*, 2002, **11**, 366–374.
19. L. Gránásy, T. Pusztai, J. A. Warren, J. F. Douglas, T. Borzsonyi and V. Ferreiro: *Nat. Mater.*, 2003, **2**, 92–96.
20. M. F. Zhu, S. Y. Lee and C. P. Hong: *Phys. Rev. E*, 2004, **69E**, 061610.